Negative-parity nucleon excited state in nuclear matter

Keisuke Ohtani,[1,][*] Philipp Gubler,[2] and Makoto Oka[1,3]

[1]*Department of Physics, H-27, Tokyo Institute of Technology, Meguro, Tokyo 152-8551, Japan*
[2]*Institute of Physics and Applied Physics, Yonsei University, Seoul 120-749, Korea*
[3]*Advanced Science Research Center, Japan Atomic Energy Agency, Tokai, Ibaraki 319-1195, Japan*

Spectral functions of the nucleon and its negative-parity excited state in nuclear matter are studied by using QCD sum rules and the maximum entropy method (MEM). It is found that in-medium modifications of the spectral functions are attributed mainly to density dependencies of the $\langle \bar{q}q \rangle$ and $\langle q^{\dagger}q \rangle$ condensates. The MEM reproduces the lowest-energy peaks of both the positive- and negative-parity nucleon states at finite density up to $\rho \sim \rho_N$ (normal nuclear matter density). As the density grows, the residue of the nucleon ground state decreases gradually while the residue of the lowest negative-parity excited state increases slightly. On the other hand, the positions of the peaks, which correspond to the total energies of these states, are almost density independent for both parity states. The density dependencies of the effective masses and vector self-energies are also extracted by assuming phenomenological mean-field-type propagators for the peak states. We find that, as the density increases, the nucleon effective mass decreases while the vector self-energy increases. The density dependence of these quantities for the negative-parity state on the other hand turns out to be relatively weak.

I. INTRODUCTION

The question of how nucleons behave in dense matter is of great importance both from the point of view of nuclear physics and QCD. In particular, the role played by the partial restoration of chiral symmetry in nuclear matter and its influence on properties of the nucleonic ground and excited states has attracted continued interest. In this context, it is especially worth mentioning the potential medium modifications of the negative-parity nucleon state, which are interesting from the viewpoint of the chiral symmetry and η mesic nuclei. Considering the relation between chiral symmetry and the spectral functions of chiral partners, the symmetry requires their spectral functions to be degenerate if chiral symmetry is restored. Chiral partners among hadronic states as well as hadronic spectral functions have been discussed already a long time ago [1]. Assuming that the chiral partner of the positive-parity nucleon ground state N(939) is the lowest lying negative-parity state N(1535), the relation between the restoration of chiral symmetry and the modifications of N(939) and N(1535) has been investigated within effective models such as linear sigma models [2,3]. These studies show that two assignments; namely, the naive and mirror assignments, of the chiral transformation to the chiral partners lead to different characteristic modifications of the physical nucleon states at finite density.

Potentially η nuclear systems, so-called η-mesic nuclei, were first investigated by Haider and Liu [4]. The formation of η-mesic nuclei is strongly related to in-medium modifications of N(939) and N(1535) since the ηN system strongly couples to N(1535) and its threshold is close to the mass of N(1535). Such nuclei have been studied both in theoretical [5–8] and experimental approaches [9–11]. The studies of

meson-nucleus bound systems are interesting because the hadron properties at finite density, which are related to the restoration of spontaneous breaking of the chiral symmetry, can be investigated in laboratories.

In this paper, we study the spectral functions of both the positive and negative-parity nucleons in nuclear matter by using QCD sum rules. This method was initially developed and applied to the investigation of the meson properties in vacuum by Shifman *et al.* [12,13]. It was subsequently used to study baryonic channels by Ioffe [14]. Especially for the nucleon, the analyses were thereafter continuously improved over the years by including higher-order terms in the perturbative Wilson coefficients [15–20] or nonperturbative power corrections [16,21,22]. Additionally, it was pointed out that the nucleon operator couples to both positive and negative-parity states [23]. The combined contributions of these states make the analysis complicated and especially spoil the result of the negative-parity states. This difficulty can be remedied by the methods of parity projection, which were proposed by Jido *et al.* [24] and Kondo *et al.* [25]. In these studies, the α_s corrections, which are large for the nucleon channel, were not considered. To include these α_s corrections in the parity-projected sum rules, the present authors have improved the parity projection for baryonic QCD sum rules and studied the masses of both positive-parity and negative-parity nucleon states in vacuum [26].

QCD sum rules have also been used to investigate hadron properties in nuclear matter [27–29]. The generalization of nucleonic QCD sum rules in nuclear matter was first proposed by Drukarev [30]. Since then, many studies have been carried out for the medium modifications of its energy, effective mass, and vector self-energy, which characterize properties of the nucleon in nuclear matter [31,32]. However, all previous studies have so far focused only on the positive-parity state N(939).

[*]ohtani.k@th.phys.titech.ac.jp

In this work, we apply the parity-projected nucleon QCD sum rule with the phase-rotated Gaussian kernel, which was already used for the vacuum [26], to the analyses in nuclear matter. Properties of the nucleon and its negative-parity excited state are extracted from the sum rules with the help of the maximum entropy method (MEM). The MEM analysis combined with QCD sum rules can provide the most probable spectral function without any strong constraint on its form and has so far been successfully applied to the ρ meson vacuum channel [33], the nucleon vacuum channel [26,34], and others [35–37]. Assuming the peaks in the spectral functions to be described by in-medium nucleon propagators, we furthermore investigate the density dependence of the effective masses and vector self-energies of both the nucleon ground state and its negative parity first-excited state.

The paper is organized as follows: In Sec. II, we construct the parity-projected in-medium nucleon QCD sum rules and discuss the behavior of the resulting equations. The results of the analyses are summarized in Sec. III where the density dependence of the spectral functions of both positive- and negative-parity states, the effective masses, and the vector self-energies are presented. Next, effects of the uncertainties of the condensates and their in-medium behavior on the results are studied in Sec. IV. We additionally discuss the validity of the parity projection at finite spatial momentum in the same section. Summary and conclusions are given in Sec. V.

II. PARITY-PROJECTED NUCLEON QCD SUM RULE IN NUCLEAR MATTER

A. Parity projection of nucleon QCD sum rules in nuclear matter

The parity-projected QCD sum rules are constructed from the "forward-time" correlation function [24]

$$
\Pi_m(q_0,|\vec{q}|) = i \int d^4x\, e^{iqx}\theta(x_0)
$$
$$
\times \langle \Psi_0(\rho,u^\mu)|T[\eta(x)\bar{\eta}(0)]|\Psi_0(\rho,u^\mu)\rangle, \quad (1)
$$

where $\eta(x)$ is the nucleon interpolating field and $|\Psi_0(\rho,u^\mu)\rangle$ represents the ground state of nuclear matter, which is characterized by its velocity u^μ and the nucleon density ρ. We assume that $|\Psi_0(\rho,u^\mu)\rangle$ is invariant under parity and time-reversal transformations. In the rest frame of nuclear matter, the velocity is given by $u^\mu = (1,\vec{0})$. Note that, in Ref. [24], this correlator was called the "old-fashioned" correlator. The essential difference from the time-ordered correlation function is the insertion of the Heaviside step function $\theta(x_0)$ before carrying out the Fourier transform. This correlator contains contributions only from states which propagate forward in time. With the help of the Lorentz covariance, parity invariance and time reversal invariance of the nuclear matter ground state, the correlation function can be decomposed into three components [31]:

$$
\Pi_m(q_0,|\vec{q}|) = \slashed{q}\,\Pi_{m1}(q_0,|\vec{q}|) + \Pi_{m2}(q_0,|\vec{q}|)
$$
$$
+ \slashed{u}\,\Pi_{m3}(q_0,|\vec{q}|). \quad (2)
$$

The scalar functions Π_{m1}, Π_{m2}, and Π_{m3} depend on two scalar variables q^2 and $q \cdot u$. In what follows, we denote $(q^2, q \cdot u)$ as

$(q_0,|\vec{q}|)$ since we only work in the rest frame of nuclear matter. Note that Π_{m1}, Π_{m2}, and Π_{m3} contain information about the in-medium properties of both positive- and negative-parity states because replacing the operator $\eta(x) \to \gamma_5\eta(x)$ only changes the sign of Π_{m2}.

To separate these positive- and negative-parity contributions, we multiply the parity projection operators $P^\pm = \frac{\gamma_0 \pm 1}{2}$ to the correlator, take the trace over the spinor index and thus obtain the parity-projected correlation functions:

$$
\Pi_m^+(q_0,|\vec{q}|) \equiv q_0\Pi_{m1}(q_0,|\vec{q}|) + \Pi_{m2}(q_0,|\vec{q}|) + u_0\Pi_{m3}(q_0,|\vec{q}|),
$$
$$
\Pi_m^-(q_0,|\vec{q}|) \equiv q_0\Pi_{m1}(q_0,|\vec{q}|) - \Pi_{m2}(q_0,|\vec{q}|) + u_0\Pi_{m3}(q_0,|\vec{q}|).
$$
$$(3)$$

Note that the parity projection can be carried out in accordance with that in vacuum because it is based on the invariance of the ground state of nuclear matter under parity transformation.

QCD sum rules are relations between correlators computed in different regions of q_0. Specifically, $\Pi_{m\text{OPE}}^\pm$, which is calculated at a large $-q_0^2$ by the operator product expansion (OPE), and the spectral function $\rho_m^\pm \equiv \frac{1}{\pi}\text{Im}[\Pi_m^\pm]$ at $q_0 > 0$ can be related. By making use of the analyticity of the correlation function, one can construct the parity-projected QCD sum rules:

$$
\int_{-\infty}^{\infty} \text{Im}[\Pi_{m\text{OPE}}^\pm(q_0,|\vec{q}|)]W(q_0)dq_0
$$
$$
= \pi \int_0^\infty \rho_m^\pm(q_0,|\vec{q}|)W(q_0)dq_0. \quad (4)
$$

Here we have introduced a weighting function $W(q_0)$, which is real at real q_0 and analytic in the upper half of the imaginary plane of q_0. The details of the derivation of Eq. (4) are discussed in Ref. [26].

B. Operator product expansion in nuclear matter

In this section, we provide the explicit form of $\Pi_{m\text{OPE}}^\pm$, including all known α_s corrections. For the nucleon, there are two independent local interpolating operators:

$$
\eta_1(x) = \epsilon^{abc}[u^{Ta}(x)C\gamma_5 d^b(x)]u^c(x), \quad (5)
$$

$$
\eta_2(x) = \epsilon^{abc}[u^{Ta}(x)Cd^b(x)]\gamma_5 u^c(x). \quad (6)
$$

Here, a, b, and c are color indices, $C = i\gamma_0\gamma_2$ stands for the charge-conjugation matrix, while the spinor indices are omitted for simplicity. A general interpolating field can be expressed as

$$
\eta(x) = \eta_1(x) + \beta\eta_2(x), \quad (7)
$$

where β is a real parameter. The choice $\beta = -1$ is called the Ioffe current, which is widely used in sum-rule analyses studying the nucleon ground state. It is straightforward to obtain the imaginary part of the forward-time correlator of Eq. (1) from the time-ordered correlator given in the literature

[18,26,38]. The explicit expressions are given as

$$\frac{1}{\pi}\mathrm{Im}[q_0\Pi_{m1\mathrm{OPE}}(q_0,|\vec{q}|)]$$

$$= \frac{C_1}{2^{11}\pi^4}\left\{1+\frac{\alpha_s}{\pi}\left[\frac{71}{12}-\ln\left(\frac{q^2}{\mu^2}\right)\right]\right\}q_0(q^2)^2\theta(q_0-|\vec{q}|) + \frac{C_1}{2^{10}\pi^2}\left\langle\frac{\alpha_s}{\pi}G^2\right\rangle_m q_0\,\theta(q_0-|\vec{q}|) - \frac{C_1}{2^5 3^2\pi^2}\langle q^\dagger iD_0 q\rangle_m$$

$$\times[5q_0\theta(q_0-|\vec{q}|)-4|\vec{q}|^2\delta(q_0-|\vec{q}|)] - \frac{C_1}{2^9 3^2\pi^2}\left\langle\frac{\alpha_s}{\pi}(E^2+B^2)\right\rangle_m[q_0\theta(q_0-|\vec{q}|)-2|\vec{q}|^2\delta(q_0-|\vec{q}|)]$$

$$+\frac{1}{2^4 3}\left(C_2+\frac{\alpha_s}{\pi}C_3\right)\langle\bar{q}q\rangle_m^2\delta(q_0-|\vec{q}|) - \frac{C_4}{2^3 3\pi}\frac{\alpha_s}{\pi}\langle\bar{q}q\rangle_m^2$$

$$\times\mathrm{Im}\left[\ln(2|\vec{q}|)\frac{|\vec{q}|}{(q_0+i\epsilon)^2-|\vec{q}|^2}+\ln(|\vec{q}|-(q_0+i\epsilon))\frac{q_0}{(q_0+i\epsilon)^2-|\vec{q}|^2}\right]$$

$$+\frac{C_1}{2^4 3}\langle q^\dagger q\rangle_m^2\delta(q_0-|\vec{q}|) - \frac{C_1}{2^5 3\pi^2}\langle q^\dagger q\rangle_m q_0^2\,\theta(q_0-|\vec{q}|) - \frac{1}{2^5 3\pi^2}\left[C_5-C_1\ln\left(\frac{q^2}{\mu^2}\right)\right]\frac{\alpha_s}{\pi}\langle q^\dagger q\rangle_m q_0^2\,\theta(q_0-|\vec{q}|)$$

$$-\frac{C_6}{2^5 3^2\pi^2}\langle q^\dagger g\sigma\cdot Gq\rangle_m\frac{|\vec{q}|}{2}\delta(q_0-|\vec{q}|) - \frac{C_1}{2^4 3\pi^2}\left[\langle q^\dagger iD_0 iD_0 q\rangle_m+\frac{1}{12}\langle q^\dagger g\sigma\cdot Gq\rangle_m\right]$$

$$\times\left(-2|\vec{q}|\delta(q_0-|\vec{q}|)+2|\vec{q}|^4\mathrm{Im}\left[\frac{1}{4\pi|\vec{q}|^2-i\epsilon}\frac{1}{(q_0-|\vec{q}|+i\epsilon)^2}\right]\right), \tag{8}$$

$$\frac{1}{\pi}\mathrm{Im}[\Pi_{m2\mathrm{OPE}}(q_0,|\vec{q}|)]$$

$$= -\frac{1}{2^6\pi^2}\left(C_2+C_7\frac{\alpha_s}{\pi}\right)\langle\bar{q}q\rangle_m q^2\theta(q_0-|\vec{q}|) + \frac{3C_8}{2^6\pi^2}\langle\bar{q}g\sigma\cdot Gq\rangle_m\,\theta(q_0-|\vec{q}|) - \frac{C_9}{6\pi^2}\left[\langle\bar{q}iD_0 iD_0 q\rangle_m+\frac{1}{8}\langle\bar{q}g\sigma\cdot Gq\rangle_m\right]$$

$$\times\frac{|\vec{q}|}{2}\delta(q_0-|\vec{q}|) + \frac{C_2}{2^5\pi^2}\langle\bar{q}iD_0 q\rangle_m q_0\theta(q_0-|\vec{q}|) + \frac{C_2}{2^3 3}\langle\bar{q}q\rangle_m\langle q^\dagger q\rangle_m\,\delta(q_0-|\vec{q}|), \tag{9}$$

$$\frac{1}{\pi}\mathrm{Im}[\Pi_{m3\mathrm{OPE}}(q_0,|\vec{q}|)]$$

$$= \frac{5C_1}{2^3 3^2\pi^2}\langle q^\dagger iD_0 q\rangle_m q_0\theta(q_0-|\vec{q}|) + \frac{C_1}{2^7 3^2\pi^2}\left\langle\frac{\alpha_s}{\pi}(E^2+B^2)\right\rangle_m q_0\theta(q_0-|\vec{q}|) + \frac{C_1}{2^3 3}\langle q^\dagger q\rangle_m^2\,\delta(q_0-|\vec{q}|)$$

$$-\frac{C_1}{2^4 3\pi^2}\langle q^\dagger q\rangle_m(q_0^2-|\vec{q}|^2)\,\theta(q_0-|\vec{q}|) - \frac{1}{2^4 3\pi^2}\left[C_{10}-C_1\ln\left(\frac{q^2}{\mu^2}\right)\right]\frac{\alpha_s}{\pi}\langle q^\dagger q\rangle_m(q_0^2-|\vec{q}|^2)\theta(q_0-|\vec{q}|)$$

$$+\frac{C_6}{2^6 3\pi^2}\langle q^\dagger g\sigma\cdot Gq\rangle_m\theta(q_0-|\vec{q}|) - \frac{C_1}{2^3\pi^2}\left[\langle q^\dagger iD_0 iD_0 q\rangle_m+\frac{1}{12}\langle q^\dagger g\sigma\cdot Gq\rangle_m\right]\frac{|\vec{q}|}{2}\delta(q_0-|\vec{q}|), \tag{10}$$

where $q^2=q_0^2-\vec{q}^{\,2}$ and the coefficients C_i are defined as

$$C_1=5+2\beta+5\beta^2,\quad C_2=7-2\beta-5\beta^2,\quad C_3=\frac{325}{18}+\frac{448}{9}\beta+\frac{511}{18}\beta^2,\quad C_4=\frac{47}{3}-\frac{10}{3}\beta-\frac{61}{3}\beta^2,$$

$$C_5=\frac{49}{3}+\frac{14}{3}\beta+\frac{49}{3}\beta^2,\quad C_6=7+10\beta+7\beta^2,\quad C_7=\frac{15}{2}-3\beta-\frac{9}{2}\beta^2,\quad C_8=1-\beta^2,$$

$$C_9=2-\beta-\beta^2,\quad C_{10}=\frac{211}{12}+\frac{31}{6}\beta+\frac{211}{12}\beta^2. \tag{11}$$

The matrix elements $\langle\mathcal{O}\rangle_m$ stand for the expectation value of operators $\mathcal{O}$ in nuclear matter.

C. QCD condensates at finite nucleon density

The correlation functions are characterized by in-medium QCD condensates. While the value of the vector quark condensate $\langle q^\dagger q\rangle_m$ at density ρ is $\frac{3}{2}\rho$ exactly, the other condensates are not precisely determined and their density dependencies may be more complicated. In this paper, we estimate their values in the linear density approximation, which is valid at sufficiently low density [30,39]. The in-medium condensates $\langle\mathcal{O}\rangle_m$ are in this approximation expressed as $\langle\mathcal{O}\rangle_m=\langle\mathcal{O}\rangle_0+\rho\langle\mathcal{O}\rangle_N$ with the

vacuum condensates $\langle \mathcal{O} \rangle_0$ and the nucleon matrix elements $\langle \mathcal{O} \rangle_N \equiv \langle N | \mathcal{O} | N \rangle$. Each matrix element is evaluated as follows:

$$\langle \overline{q}q \rangle_m = \langle \overline{q}q \rangle_0 + \rho \langle \overline{q}q \rangle_N = \langle \overline{q}q \rangle_0 + \rho \frac{\sigma_N}{2m_q}, \quad \langle q^\dagger q \rangle_m = \rho \frac{3}{2}, \quad \left\langle \frac{\alpha_s}{\pi} G^2 \right\rangle_m = \left\langle \frac{\alpha_s}{\pi} G^2 \right\rangle_0 + \rho \left\langle \frac{\alpha_s}{\pi} G^2 \right\rangle_N,$$

$$\langle q^\dagger i D_0 q \rangle_m = \rho \langle q^\dagger i D_0 q \rangle_N = \rho \frac{3}{8} M_N A_2^q, \quad \left\langle \frac{\alpha_s}{\pi} (E^2 + B^2) \right\rangle_m = \rho \left\langle \frac{\alpha_s}{\pi} (E^2 + B^2) \right\rangle_N = \rho \frac{3}{2\pi} M_N \alpha_s(\mu^2) A_2^g,$$

$$\langle \overline{q} i D_0 q \rangle_m = m_q \langle q^\dagger q \rangle_m \simeq 0, \quad \langle \overline{q} g \sigma \cdot G q \rangle_m = \langle \overline{q} g \sigma \cdot G q \rangle_0 + \rho \langle \overline{q} g \sigma \cdot G q \rangle_N \approx m_0^2 \langle \overline{q}q \rangle_m,$$

$$\langle q^\dagger g \sigma \cdot G q \rangle_m = \rho \langle q^\dagger g \sigma \cdot G q \rangle_N,$$

$$\langle q^\dagger i D_0 i D_0 q \rangle_m + \frac{1}{12} \langle q^\dagger g \sigma \cdot G q \rangle_m = \left(\langle q^\dagger i D_0 i D_0 q \rangle_N + \frac{1}{12} \langle q^\dagger g \sigma \cdot G q \rangle_N \right) \rho = \rho \frac{1}{4} M_N^2 A_3^q,$$

$$\langle \overline{q} i D_0 i D_0 q \rangle_{\rho_N} + \frac{1}{8} \langle \overline{q} g \sigma \cdot G q \rangle_m = \left(\langle \overline{q} i D_0 i D_0 q \rangle_N + \frac{1}{8} \langle \overline{q} g \sigma \cdot G q \rangle_N \right) \rho = \rho \frac{3}{4} M_N^2 e_2, \tag{12}$$

where E and B are the color electric and color magnetic fields, respectively. $\langle \overline{q}q \rangle$ denotes the averages over up and down quarks, $\frac{1}{2}(\langle \overline{u}u \rangle + \langle \overline{d}d \rangle)$.

The quantities A_2^q, A_2^g, A_3^q, e_2 can be expressed as moments of the parton distribution functions [31]. The values of the parameters appearing in Eq. (12) are given in Table I. The uncertainties of the values of m_q and σ_N will be discussed in Sec. IV. Note that the higher-order density terms of the chiral condensate $\langle \overline{q}q \rangle$ have been computed by using chiral perturbation theory [40,41]. These contributions are, however, small up to the normal nuclear mater density and thus we do not take them into account in this study.

D. Phase-rotated Gaussian QCD sum rules

To explicitly compute both the left- and right-hand sides of Eq. (4), we have to specify the kernel $W(q_0)$. In a previous study, in which the nucleon properties in vacuum were investigated [26], we tested several kinds of kernels, such as the Borel and Gaussian kernels, and found that the phase-rotated Gaussian kernel is most suitable for studying the nucleon ground state and its negative-parity excitation. As it was pointed out in Ref. [26], by choosing an appropriate phase parameter θ, the kernel improves the convergence of the OPE

and at the same time suppresses the α_s corrections. Moreover, the four-quark condensate contributions are suppressed with this kernel, and therefore the uncertainties caused by the four-quark condensates, whose values are only weakly constrained, will not seriously affect the results of the QCD sum rule analysis.

We will later carry out the sum-rule analysis for the nucleon at rest relative to nuclear matter and also at the Fermi surface. There is no guarantee that the above desirable features are kept when investigating the in-medium nucleon properties at finite $|\vec{q}|$. We, in fact, find that the suppression of the contributions from the α_s corrections becomes less effective as $|\vec{q}|$ increases. Therefore, we improve the phase-rotated kernel $W(q_0, |\vec{q}|)$ as

$$W(s, \tau, \theta, q_0, |\vec{q}|)$$
$$= \frac{1}{\sqrt{4\pi\tau}} \frac{1}{2} \left[(q_0 - |\vec{q}|) e^{-2i\theta} \exp \left(-\frac{(q^2 e^{-2i\theta} - s)^2}{4\tau} \right) \right.$$
$$\left. + (q_0 - |\vec{q}|) e^{2i\theta} \exp \left(-\frac{(q^2 e^{2i\theta} - s)^2}{4\tau} \right) \right]. \tag{13}$$

s, τ, and θ are parameters in our QCD sum rule and whose analyzed parameter regions will be discussed in the next section. For $|\vec{q}| = 0$, the above kernel is equivalent to that used previously in Ref. [26].

Substituting Eqs. (8)–(10) and (13) into Eq. (4), we finally obtain the parity-projected nucleon QCD sum rules as

$$G_{mOPE}^\pm(s, \tau, \theta)$$
$$\equiv \int_{-\infty}^{\infty} \frac{1}{\pi} \mathrm{Im}[\Pi_{mOPE}^\pm(q_0, |\vec{q}|)] W(s, \tau, \theta, q_0, |\vec{q}|) dq_0$$
$$= G_{m1OPE}(s, \tau, \theta) \pm G_{m2OPE}(s, \tau, \theta) + G_{m3OPE}(s, \tau, \theta)$$
$$= \int_0^{\infty} \rho_m^\pm(q_0) W(s, \tau, \theta, q_0, |\vec{q}|) dq_0. \tag{14}$$

Here, $G_{miOPE}(s, \tau, \theta)$ $(i = 1, 2, 3)$ are defined as

$$G_{m1OPE}(s, \tau, \theta)$$
$$= \int_{-\infty}^{\infty} \mathrm{Im} \left[\frac{q_0 \Pi_{m1OPE}(q_0, |\vec{q}|)}{\pi} \right] W(s, \tau, \theta, q_0, |\vec{q}|) dq_0,$$

TABLE I. Values of parameters appearing in Eq. (12).

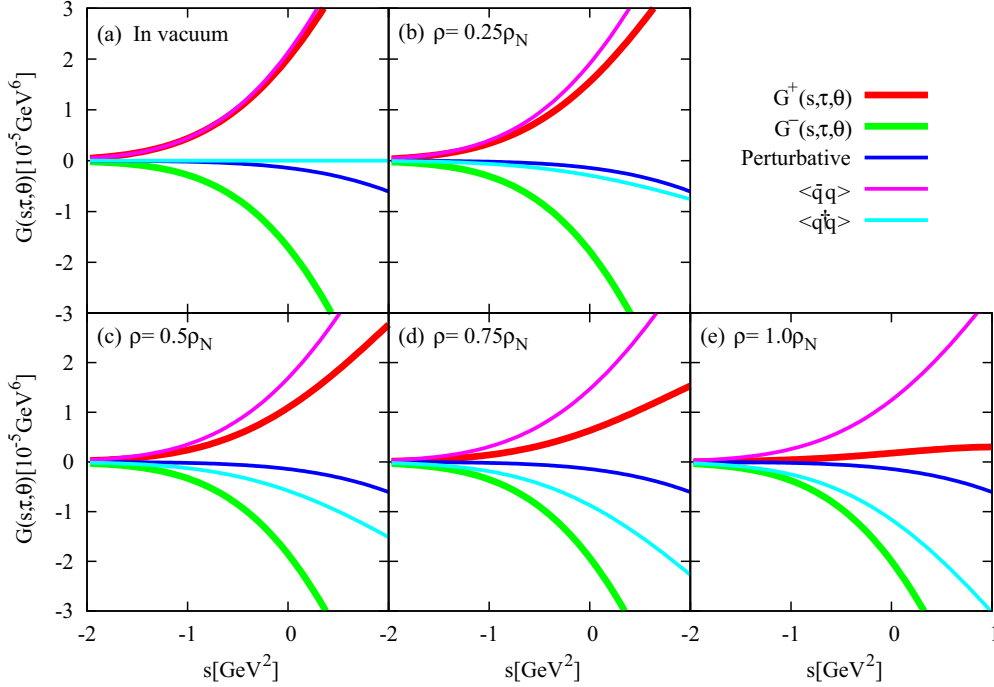| Parameter	Value
$\langle \overline{q}q \rangle_0$	$-(0.246 \pm 0.002 \text{ GeV})^3$ [42]
m_q	4.725 MeV [43]
σ_N	45 MeV
$\langle q^\dagger q \rangle_m$	$\rho \frac{3}{2}$
$\left\langle \frac{\alpha_s}{\pi} G^2 \right\rangle_0$	$0.012 \pm 0.0036 \text{ GeV}^4$ [44]
$\left\langle \frac{\alpha_s}{\pi} G^2 \right\rangle_N$	$-0.65 \pm 0.15 \text{ GeV}$ [45]
A_2^q	0.62 ± 0.06 [46]
A_2^g	0.359 ± 0.146 [46]
A_3^q	0.15 ± 0.02 [46]
e_2	0.017 ± 0.047 [47]
m_0^2	$0.8 \pm 0.2 \text{ GeV}^2$ [44]
$\langle q^\dagger g \sigma \cdot G q \rangle_N$	-0.33 GeV^2 [45]

FIG. 1. The density dependence of $G^{\pm}_{m\mathrm{OPE}}(s,\tau,\theta)$. The perturbative, chiral condensate $\langle\overline{q}q\rangle$, vector quark condensate $\langle q^{\dagger}q\rangle$ terms and the total are shown at $\tau = 0.5$ GeV^4, $\beta = -0.9$, $\theta = 0.108\pi$, and $|\vec{q}| = 0$. The $\langle q^{\dagger}q\rangle$ term stands for the sum of the terms proportional to the condensate $\langle q^{\dagger}q\rangle$ in $G_{m1\mathrm{OPE}}(s,\tau,\theta)$ and $G_{m3\mathrm{OPE}}(s,\tau,\theta)$.

$$G_{m2\mathrm{OPE}}(s,\tau,\theta)$$
$$= \int_{-\infty}^{\infty} \mathrm{Im}\left[\frac{\Pi_{m2\mathrm{OPE}}(q_0,|\vec{q}|)}{\pi}\right] W(s,\tau,\theta,q_0,|\vec{q}|)dq_0,$$
$$G_{m3\mathrm{OPE}}(s,\tau,\theta)$$
$$= \int_{-\infty}^{\infty} \mathrm{Im}\left[\frac{\Pi_{m\mathrm{uOPE}}(q_0,|\vec{q}|)}{\pi}\right] W(s,\tau,\theta,q_0,|\vec{q}|)dq_0. \quad (15)$$

The functions $G^{\pm}_{m\mathrm{OPE}}(s,\tau,\theta)$ are shown in Fig. 1 at $\tau = 0.5$ [GeV^4], $\theta = 0.108\pi$, and $|\vec{q}| = 0$ for various densities. The qualitative behavior at finite spatial momentum is similar to that at $|\vec{q}| = 0$. In this figure, also shown are the perturbative, chiral condensate $\langle\overline{q}q\rangle$ and vector quark condensate $\langle q^{\dagger}q\rangle$ terms, which are dominant. From Eq. (14) and Fig. 1, one sees that the chiral condensate term dominates in vacuum and is responsible for the difference between $G^{+}_{m\mathrm{OPE}}$ and $G^{-}_{m\mathrm{OPE}}$. This observation shows clearly that the difference between the positive- and negative-parity spectral functions is caused by the emergence of the chiral condensate $\langle\overline{q}q\rangle$. We also find that, as the density increases, $G^{+}_{m\mathrm{OPE}}$ becomes small due to the decrease of the absolute value of $\langle\overline{q}q\rangle$ and the increase of the vector quark condensate. On the other hand, $G^{-}_{m\mathrm{OPE}}$ shows no significant change since the modifications of the $\langle\overline{q}q\rangle$ and $\langle q^{\dagger}q\rangle$ condensates cancel each other out to a large degree.

III. NUMERICAL ANALYSIS OF SUM RULES

A. Spectral functions of positive- and negative-parity states

We first discuss the parameter regions of τ, s, θ, and β used for the analyses of this work. Considering the form of $W(s,\tau,\theta,q_0,|\vec{q}|)$ in Eq. (13), we expect that, for small τ

values, $G^{\pm}_{m}(s,\tau,\theta)$ will retain traces of the peak structures of the spectral function, while at large τ, it will be dominated by continuum contributions. This is because τ represents the typical energy scale over which the kernel $W(s,\tau,\theta,q_0,|\vec{q}|)$ averages the spectral function. We therefore use several values of τ ($\tau = 0.5, 0.75, 1.0, 1.25, 1.5, 1.75, 2.0$ GeV^4) simultaneously and determine the corresponding parameter region of s for each τ. The minimum values of s at fixed τ are determined based on the criterion that the ratio of the highest-dimensional OPE term to the total $G^{\pm}_{m\mathrm{OPE}}(s,\tau,\theta)$ is less than 0.25. The maximum values of s are chosen to satisfy the condition that the second node of the kernel as a function of q_0 is less than 2.0 GeV because it is difficult to extract information in the q_0 region above this second node due to the suppression and fast oscillation of the kernel. The specific values of the minimum and maximum s for each τ are shown in Table II. The values of θ and β are set to 0.108π and -0.9 to suppress the effects of higher-order α_s corrections and uncertainties of condensates, respectively. For more details about the parameter determination, we refer the reader to Ref. [26].

TABLE II. Values of $s_{\mathrm{min/max}}$ [GeV^2] at $\beta = -0.9$ and fixed τ [GeV^4].

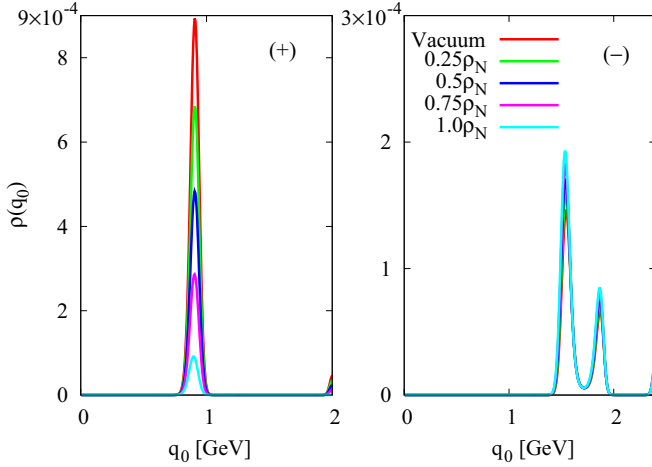| τ	0.5	0.75	1.0	1.25	1.5	1.75	2.0
s_{min} of G^{+}_{m}	−2.44	−3.92	−5.41	−6.90	−8.39	−9.88	−11.37
s_{max} of G^{+}_{m}	0.90	−0.10	−1.20	−2.20	−3.40	−4.50	−5.70
s_{min} of G^{-}_{m}	−1.27	−2.26	−3.27	−4.28	−5.30	−6.32	−7.35
s_{max} of G^{-}_{m}	0.90	−0.10	−1.20	−2.20	−3.40	−4.50	−5.70

FIG. 2. The positive- (left) and negative-parity (right) spectral functions extracted from $G^{\pm}_{m\mathrm{OPE}}(s,\tau,\theta)$ of Eq. (14) by MEM. The red, green, blue, magenta, and light blue lines correspond to the spectral functions at the density $0.0\rho_N$, $0.25\rho_N$, $0.5\rho_N$, $0.75\rho_N$, and $1.0\rho_N$, respectively. Here ρ_N denotes the normal nuclear matter density.

We apply the maximum entropy method (MEM) to the OPE data of Eq. (14) and extract the spectral functions of both positive and negative-parity states. The advantage of this method is that the most probable spectral function can be obtained without assuming its specific form such as the "pole + continuum" ansatz [33]. In the MEM analysis, however, we have to introduce the so-called default model $m(q_0)$, which should include our prior knowledge of the spectral function. To correctly reflect the spectral behavior both in the high- and low-energy regions, we use the following default model:

$$m(q_0) = \bar{m}(\beta) \frac{1}{1 + e^{(q_{\mathrm{th}} - q_0)/\delta}},$$

$$\bar{m}(\beta) = \frac{5 + 2\beta + 5\beta^2}{128(2\pi)^4}, \qquad (16)$$

where the values of q_{th} and δ are chosen as 3.0 GeV and 0.1 GeV, respectively. The factor $\bar{m}(\beta)$ is determined so that $m(q_0)$ agrees with the asymptotic behavior of the spectral function at high energy. For further technical details of the MEM, we refer the reader to Refs. [33,48,49]. The errors of the OPE data in vacuum $\sigma(s,\tau)_{\rho=0}$ are evaluated based on the method proposed in Ref. [50], while the errors $\sigma(s,\tau)_{\rho=\rho_N}$ in nuclear matter are determined by assuming that the relative errors are density independent, $[\sigma(s,\tau)/G_{m\mathrm{OPE}(s,\tau)}]_{\rho=\rho_N} = [\sigma(s,\tau)/G_{m\mathrm{OPE}}(s,\tau)]_{\rho=0}$.

We first analyze the in-medium spectral functions of the nucleons at rest relative to nuclear matter ($\vec{q} = 0$). The obtained spectral functions are shown in Fig. 2. For positive parity, the peak appears at about 910 MeV in vacuum. This peak corresponds to the nucleon ground state N(939). As the density increases, the height of the peak decreases while the peak position does not change much. For negative parity, two peaks appear at 1550 and 1870 MeV in vacuum. The first peak lies close to the lowest negative-parity excitation N(1535) and

thus most likely corresponds to this state. Note, however, that it is generally difficult to disentangle two adjoining peaks in a narrow region from QCD sum-rule analyses. It is therefore possible that the lowest peak contains contributions of the higher N(1650) state. The second peak is statistically less significant than the first and its position does not correspond to any known $\frac{1}{2}^-$ nucleon excited sates. This peak may therefore be a manifestation of the continuum. Consistently with the behavior of the OPE data shown in Fig. 1, the negative-parity spectral function is not modified significantly at finite density. These findings indicate that the energies of the lowest-lying states of both positive and negative parity are almost density independent while the coupling strength of the employed interpolating field to the N(939) state decreases as the density increases.

B. Estimation of self energies

So far, we have found that the peak positions; namely, the total energies of the nucleon and its negative-parity excited state, are not sensitive to matter effects up to nuclear matter density. The behavior of the nucleon ground state is consistent with the small binding energy per nucleon of nuclear matter. The results for the negative-parity state are, on the other hand, unexpected because one would naively anticipate that its peak moves towards the peak of the positive-parity spectral function as the chiral symmetry is partially restored in the nuclear medium.

The quantum hadrodynamics (QHD) model has been successfully applied to the investigation of nuclei and in-medium nucleon properties [51,52]. In this framework, the nearly density-independent single-particle energy of the nucleon in nuclei is caused by the cancellation of the scalar and vector self-energies. The investigation of the self-energies of the negative-parity state, to be carried out in this section within our QCD sum-rule approach, will hence be similarly helpful to comprehend its remarkable behavior.

Consider the nucleon propagator in nuclear matter,

$$G(q_0, |\vec{q}|) = \frac{Z'(q_0, |\vec{q}|)}{\slashed{q} - M - \Sigma(q_0, |\vec{q}|) + i\epsilon}, \qquad (17)$$

where $\Sigma(q_0, |\vec{q}|)$ is the nucleon self-energy and $Z'(q_0, |\vec{q}|)$ means the renormalization factor of the nucleon wave function. As in Eq. (2), the self-energy can be decomposed as

$$\Sigma(q) = \Sigma^{s'}(q_0, |\vec{q}|) + \Sigma^{v'}(q_0, |\vec{q}|)\, \slashed{u} + \Sigma^{q'}(q_0, |\vec{q}|)\, \slashed{q}. \quad (18)$$

It turns out to be convenient to redefine the quantities $\Sigma^{q'}$ to $\Sigma^{s'}$, $\Sigma^{v'}$, and Z' as

$$M^* \equiv \frac{M + \Sigma^{s'}(q_0, |\vec{q}|)}{1 - \Sigma^{q'}} = M + \Sigma^s(q_0, |\vec{q}|),$$

$$\Sigma^v(q_0, |\vec{q}|) \equiv \frac{\Sigma^{v'}(q_0, |\vec{q}|)}{1 - \Sigma^{q'}}, \qquad (19)$$

$$Z(q_0, |\vec{q}|) \equiv \frac{Z'(q_0, |\vec{q}|)}{1 - \Sigma^{q'}},$$

after which the nucleon propagator can be described as

$$G(q_0, |\vec{q}|) = Z(q_0, |\vec{q}|) \frac{\not{q} - \not{v}\Sigma_v + M^*}{(q_0 - E + i\epsilon)(q_0 + \overline{E} - i\epsilon)}, \quad (20)$$

where

$$E = \Sigma_v + \sqrt{M^{*2} + \vec{q}^{\,2}}, \quad \overline{E} = -\Sigma_v + \sqrt{M^{*2} + \vec{q}^{\,2}}. \quad (21)$$

Now we assume that the phenomenological side of the nucleon correlation function is constituted of several sharp (zero-width) positive- and negative-parity states and the continuum. Then, each scalar function of the forward-time correlation function can be expressed by a sum of the contributions from the individual states as

$$q_0 \Pi_{m1}(q_0, |\vec{q}|) = \sum_n |\lambda_n^+|^2 \frac{E_n^+}{2\sqrt{M_{n+}^{*2} + \vec{q}^{\,2}}} \frac{1}{q_0 - E_n^+ + i\epsilon} + |\lambda_n^-|^2 \frac{E_n^-}{2\sqrt{M_{n-}^{*2} + \vec{q}^{\,2}}} \frac{1}{q_0 - E_n^- + i\epsilon} + \cdots, \quad (22)$$

$$\Pi_{m2}(q_0, |\vec{q}|) = \sum_n |\lambda_n^+|^2 \frac{M_{n+}^*}{2\sqrt{M_{n+}^{*2} + \vec{q}^{\,2}}} \frac{1}{q_0 - E_n^+ + i\epsilon} - |\lambda_n^-|^2 \frac{M_{n-}^*}{2\sqrt{M_{n-}^{*2} + \vec{q}^{\,2}}} \frac{1}{q_0 - E_n^- + i\epsilon} + \cdots, \quad (23)$$

$$\Pi_{m3}(q_0, |\vec{q}|) = \sum_n |\lambda_n^+|^2 \frac{-\Sigma_{n+}^v}{2\sqrt{M_{n+}^{*2} + \vec{q}^{\,2}}} \frac{1}{q_0 - E_n^+ + i\epsilon} + |\lambda_n^-|^2 \frac{-\Sigma_{n-}^v}{2\sqrt{M_{n-}^{*2} + \vec{q}^{\,2}}} \frac{1}{q_0 - E_n^- + i\epsilon} + \cdots, \quad (24)$$

where $|\lambda_n^\pm|^2$ are the residues of the nth states. The phenomenological side of the parity-projected correlation functions can thus be expressed as follows:

$$\Pi_m^\pm(q_0, |\vec{q}|) = \sum_n \frac{|\lambda_n^\pm|^2}{2\sqrt{M_{n\pm}^{*2} + \vec{q}^{\,2}}} \frac{\left(\sqrt{M_{n\pm}^{*2} + \vec{q}^{\,2}} + M_{n\pm}^*\right)}{q_0 - E_n^\pm + i\epsilon} + \frac{|\lambda_n^\mp|^2}{2\sqrt{M_{n\mp}^{*2} + \vec{q}^{\,2}}} \frac{\left(\sqrt{M_{n\mp}^{*2} + \vec{q}^{\,2}} - M_{n\mp}^*\right)}{q_0 - E_n^\mp + i\epsilon} + \cdots. \quad (25)$$

We next fit the combinations $\Pi_{m1}(q_0, |\vec{q}|) + \Pi_{m2}(q_0, |\vec{q}|)$, $\Pi_{m1}(q_0, |\vec{q}|) - \Pi_{m2}(q_0, |\vec{q}|)$, and $\Pi_{m3}(q_0, |\vec{q}|)$ to the respective OPE functions to extract the effective masses $M_\pm^{*2}$ and the vector self-energies $\Sigma_\pm^v$. To be more precise, we substitute the imaginary parts of Eqs. (22)–(24) into Eq. (15), compute the (trivial) q_0 integral, and fit the result to $G_{m1\mathrm{OPE}}(s, \tau, \theta) + G_{m2\mathrm{OPE}}(s, \tau, \theta)$, $G_{m1\mathrm{OPE}}(s, \tau, \theta) - G_{m2\mathrm{OPE}}(s, \tau, \theta)$, and $G_{m3\mathrm{OPE}}(s, \tau, \theta)$. To carry out this fit, we keep $E_0^\pm$ and $|\lambda_0^\pm|^2$ fixed to the values obtained from the MEM analysis of $G_{m\mathrm{OPE}}^\pm(s, \tau, \theta)$. Specifically, $E_0^\pm$ is taken at the energy of the peak maximum and $|\lambda_0^\pm|^2$ is obtained by integrating the spectral function in the region of the corresponding peak. The remaining parameters that need to be fit are then the factors

$$\frac{E_0^\pm + M_{0\pm}^*}{2\sqrt{M_{0\pm}^{*2} + \vec{q}^{\,2}}}, \quad -\frac{\Sigma_{0+}^v}{2\sqrt{M_{0\pm}^{*2} + \vec{q}^{\,2}}},$$

from which we can extract the effective masses and vector self-energies.

In the above fit, one also needs to take the continuum states [not shown in Eqs. (22)–(24)] into account. For this purpose, we regard the continuum obtained from the MEM analysis of $G_{m\mathrm{OPE}}^+(s, \tau, \theta)$ and $G_{m\mathrm{OPE}}^-(s, \tau, \theta)$ as the continuum contributions from $\Pi_{m1} + \Pi_{m2}$ and $\Pi_{m1} - \Pi_{m2}$, respectively. Concretely, we assume the $q_0 \geqslant 1050\,\mathrm{MeV}$ ($q_0 \geqslant 1750\,\mathrm{MeV}$) region to be the continuum of $\Pi_{m1} + \Pi_{m2}$ ($\Pi_{m1} - \Pi_{m2}$). We have checked that the choice of the lower boundaries has no strong effects on the fitting results. The contribution of the continuum state in Π_{m3} may furthermore be neglected because there are no perturbative contributions to this term in the high-energy limit.

The fit results are given in Fig. 3. The left figure shows the behavior for the positive-parity state. As the density increases, the effective mass decreases, while the vector self-energy increases. The values of the effective mass and vector self-energy at normal nuclear matter density are about 130 and 770 MeV, respectively. These findings are qualitatively similar to the results of the previous QCD sum-rule analyses [31,32], while the magnitude of the in-medium modifications are larger than those in Refs. [31,32]. The right figure shows
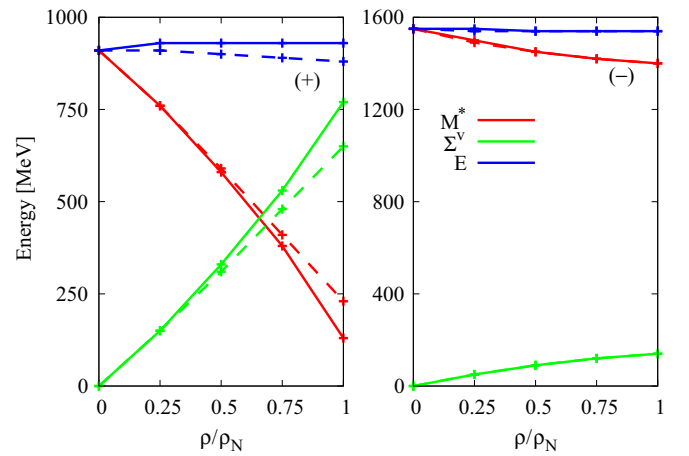

FIG. 3. The density dependence of the effective masses and vector self-energies of positive (left) and negative-parity (right) states. The red, green, and blue lines correspond to the effective masses, vector self-energies and total energies, respectively. The dashed lines are the results in which the four-quark condensate are assumed to be independent of the density (see Sec. IV A).

the negative-parity effective mass and self-energy. The density dependencies of both quantities clearly turn out to be much weaker than those of the positive-parity state.

The obtained spectral function, effective mass, and vector self-energy for the negative-parity state differ from the predictions of the chiral doublet models [2,3]. The models predict that the mass difference between the nucleon and its negative-parity excited state is reduced at finite density because it is proportional to the chiral condensate $\langle \overline{q}q \rangle$. The models furthermore predict that both the masses monotonically decrease and finally become degenerate in the chirally restored phase. Therefore, one expects in this framework that the energy of the negative-parity excited state moves towards the positive-parity state as the density increases. Our study, however, shows that the energy of the negative-parity excited state is almost density independent. The disagreement between the results of the chiral doublet model and QCD sum rules can be traced back to the $\langle q^{\dagger}q \rangle$ condensate at finite density. The cancellation between the changes of $\langle \overline{q}q \rangle$ and $\langle q^{\dagger}q \rangle$ in the medium leaves the correlation function (almost) unchanged for the negative-parity sum rule. The behavior of the negative-parity nucleon in the medium may be experimentally studied from η-mesic nuclei since their structures may be sensitive to the difference between the energies of the nucleon ground state and its first negative-parity excitation [6,7]. It will be interesting to see whether such an experiment can discriminate between the above two pictures and whether it can determine which of the two is realized in nature.

IV. DISCUSSION

In this section, we discuss the uncertainties of the in-medium condensates and their effects on the sum-rule analysis results. As we have mentioned in Sec. II B, in-medium condensates are evaluated in this work within the linear density approximation and their (linear) density dependencies are determined by the values of the quark mass, parton distribution functions, etc. The values of these quantities have some uncertainties. Furthermore, the in-medium values of the higher-order condensates such as the four-quark condensates, which are usually evaluated by using the factorization hypothesis, are poorly known because factorization can only be justified in the large-N_c limit. We also discuss the spatial momentum dependence of the results and examine the validity of the parity projection for the finite-momentum case.

A. Dependence on in-medium four-quark condensates

Four-quark condensates can, just like the chiral condensate, be related to the spontaneous breaking of chiral symmetry. Their contributions to the OPE expression of the correlation function are given in Eqs. (8)–(10). In the case of the nucleon QCD sum rules in vacuum, the four-quark condensates give the dominant nonperturbative contribution to the chiral even part $\Pi_1(q^2)$. The in-medium values of the four-quark condensates are only poorly constrained because we at present have to rely on the factorization hypothesis, according to which the four-quark condensates are given by the square of the chiral condensate. This hypothesis may not be justified

even in vacuum, while its validity at finite density is even more questionable [16,53,54]. The density dependence of the four-quark condensates and their effects on nucleon properties have been studied previously in Refs. [16,55–57], but its effect on the lowest negative-parity excited state is worked out here for the first time.

In Eqs. (8)–(10), three kinds of four-quark condensates; namely, scalar-scalar $\langle \overline{q}q \rangle^2$, scalar-vector $\langle \overline{q}q \rangle \langle q^{\dagger}q \rangle$, and vector-vector $\langle q^{\dagger}q \rangle^2$ four-quark condensates appear. Our integral kernel of Eq. (13), in fact, eliminates the contributions of $\langle \overline{q}q \rangle \langle q^{\dagger}q \rangle$ and $\langle q^{\dagger}q \rangle^2$ at leading order in α_s. The α_s corrections of these contributions are not considered in this study because the $\langle \overline{q}q \rangle \langle q^{\dagger}q \rangle$ and $\langle q^{\dagger}q \rangle^2$ condensates are not expected to have large contributions up to normal nuclear matter density, and thus their α_s corrections presumably are numerically small. We therefore study only the effects of the in-medium modification of the scalar-scalar four-quark condensates to both the positive and negative-parity nucleon states. Since only chiral-invariant four-quark condensates appear in the nucleon QCD sum rule with the Ioffe current [$\beta = -1$ in Eq. (7)] [55], one could expect that the medium modification of the $\langle \overline{q}q \rangle^2$ condensate may also be small in the vicinity of the Ioffe current (we use $\beta = -0.9$). Previous studies actually pointed out that a small density dependence of the four-quark condensate causes realistic results with a slightly decreasing total energy of the positive-parity ground state, consistent with our knowledge of nuclear phenomenology [31]. Therefore, to test this possibility, we here assume the $\langle \overline{q}q \rangle^2$ condensates to be density independent, repeat the previous analysis, and compare the two results.

This comparison is shown in Fig. 3 as the dashed lines. In these plots, we see that the density dependence of the $\langle \overline{q}q \rangle^2$ condensate mainly affects the self-energies of the positive-parity state. The density-independent four-quark condensate causes the effective mass to increase while the vector self-energy decreases. On the other hand, the behavior of the negative-parity state remains almost completely unchanged.

B. Dependence on in-medium chiral condensates

As we have seen in Fig. 1, the chiral condensate $\langle \overline{q}q \rangle_m$ term contributes dominantly to the phase-rotated QCD sum rule of the nucleon. Its density dependence at leading order in nucleon density is determined by the ratio of πN sigma term to the light quark mass, $\xi = \frac{\sigma_N}{2m_q}$ are taken as $\sigma_N = 45$ MeV, $m_q = 4.725$ MeV, and $\xi \cong 4.76$ in Sec. III. However, both σ_N and m_q have some uncertainties and these precise values are not well determined [58–65]. Especially for the σ_N value, a recent dispersion analysis of πN scattering data gives a rather large value of $\sigma_{\pi N} = (59 \pm 1.9 \pm 3.0)$ MeV [64], while another recent lattice calculation that uses quark masses at the physical point obtains a much smaller value of $\sigma_{\pi N} = 38(3)(3)$ MeV [65].

To check the dependence of the self-energies on their values, we additionally consider two cases; namely, $\xi = 3.5, 5.5$, and show the results in Fig. 4. The dependence on the factorization hypothesis for the four-quark condensates is also given in this figure. One sees that the uncertainty of ξ mainly affects the effective mass and vector self-energy of
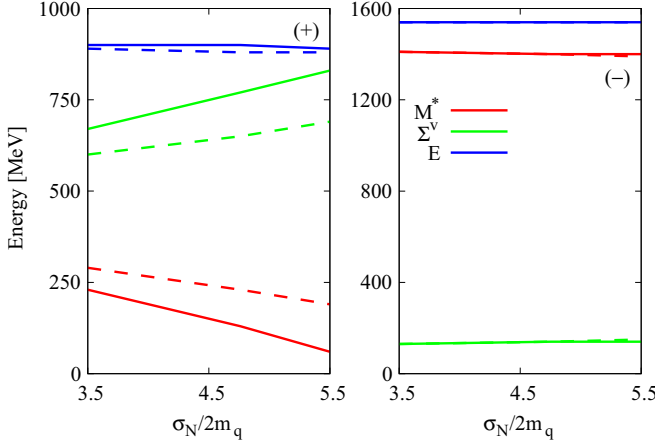
FIG. 4. The $\sigma_N/2m_q$ dependence of the effective masses and vector self-energies of positive- (left) and negative-parity (right) states. The red and green lines correspond to the effective masses and vector self-energies, respectively. The solid lines show the results with full density dependence according to the factorization hypothesis for the four-quark condensates, while the dashed lines correspond to the density-independent $\langle \overline{q}q \rangle^2$ case.
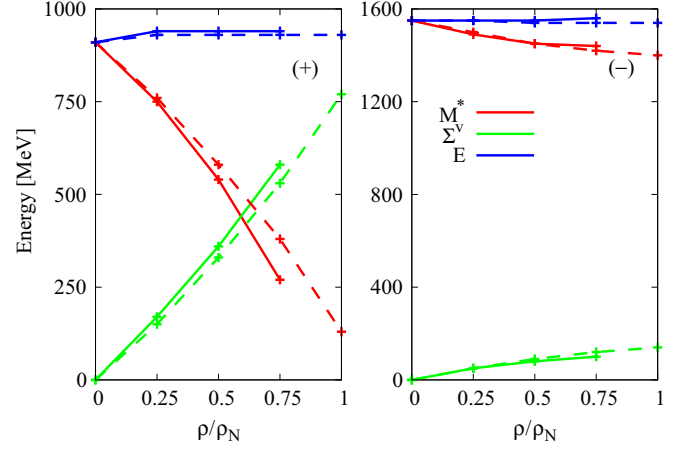

FIG. 5. The density dependence of the effective masses and vector self-energies of positive- (left) and negative-parity (right) states at the Fermi momentum. The red, green, and blue lines correspond to the effective masses, vector self-energies, and total energies, respectively. For comparison, their values at $|\vec{q}| = 0$ are shown as dashed lines.

the positive-parity state, regardless of the density dependence of the four-quark condensate. The values of the effective mass and vector self-energy at $\xi = 3.5$ and 5.5 are changed by about 100 and 70 MeV, respectively. On the other hand, the other quantities; namely, the total energies of both parity states and M^* and Σ_v of the negative-parity state, appear to be fairly insensitive to ξ. The change of ξ also affects the heights of the first peaks in the spectral functions of both the positive- and negative-parity states and thus the values of the respective residues are modified.

C. Dependence on three-dimensional momentum

As a last point, we investigate in this section the spatial momentum dependencies of the nucleon and its negative-parity excited state. In the previous sections, we have so far carried out the analyses at rest relative to nuclear matter while we shall next study the density dependence of the total energies, effective masses, and vector self-energies of both positive- and negative-parity states at the Fermi momentum $|\vec{q}_f| = (\frac{3\pi^2 \rho_N}{2})^{\frac{1}{3}}$.

The results are shown in Fig. 5 as solid lines, while the dashed lines correspond to the case of the zero spatial momentum. The momentum dependencies of the total energies, effective masses, and vector self-energies of positive and negative-parity states turn out to be small. The solid curves are not extended to the normal nuclear matter density because the MEM analysis of the positive-parity states does not work well above $\rho = 0.75\rho_N$. The reason for this failure is the rapid decrease of the ground-state residue, which is faster than for $|\vec{q}| = 0$, making it impossible to extract the positive-parity spectral function at $\rho = \rho_N$. (The lines of the negative-parity state similarly cannot be extended to the normal nuclear matter density because, when extracting the

values of the effective mass and vector self-energies, both the positive- and negative-parity spectral function are needed.) The $|\vec{q}|$ dependence of the OPE part originates from the Wilson coefficients, which depend on the two variables q^2 and $q \cdot u$. Only terms involving $q \cdot u$ lead to $|\vec{q}|$ dependencies of the in-medium spectral functions. Such contributions are small up to $0.75\rho_N$ and hence the solid and dashed curves in Fig. 5 show qualitatively the same behavior. Therefore, the weak $|\vec{q}|$ dependencies of the total energies, effective masses, and vector self-energies are consistent with the OPE side of the correlation function. To investigate the nucleon properties in more detail, higher-order contributions to the Wilson coefficients and the condensates would be needed, which is a task that goes beyond the scope of this work.

Finally, we comment on the validity of the parity projection for the nonzero-momentum case. As can be understood from Eq. (25), the parity projection can only be carried out exactly at $|\vec{q}| = 0$, meaning that $\Pi_m^{\pm}(q_0, |\vec{q}|)$ only receives contributions of states with fixed parity. On the other hand, the obtained spectral function $\rho_{m\text{Phys.}}^{\pm}(q_0, |\vec{q}| \neq 0)$ may involve some contributions of the opposite-parity states and thus the peak positions, the effective masses, and vector self-energies can in principle be affected by such mixings. The contamination can be estimated from the coefficient of the second term in Eq. (25). The ratios of the coefficient of the second term to its of first term, namely

$$\frac{\frac{|\lambda_n^{\mp}|^2}{2\sqrt{M_{n\mp}^{*2}+\vec{q}^{\,2}}} \left(\sqrt{M_{n\mp}^{*2}+\vec{q}^{\,2}} - M_{n\mp}^* \right)}{\frac{|\lambda_n^{\pm}|^2}{2\sqrt{M_{n\pm}^{*2}+\vec{q}^{\,2}}} \left(\sqrt{M_{n\pm}^{*2}+\vec{q}^{\,2}} + M_{n\pm}^* \right)},$$

are shown in Fig. 6. In this figure, one observes that, for both positive- and negative-parity states, the first term is much larger than the second and thus the mixing effect can in practice be ignored for momenta around the Fermi surface.
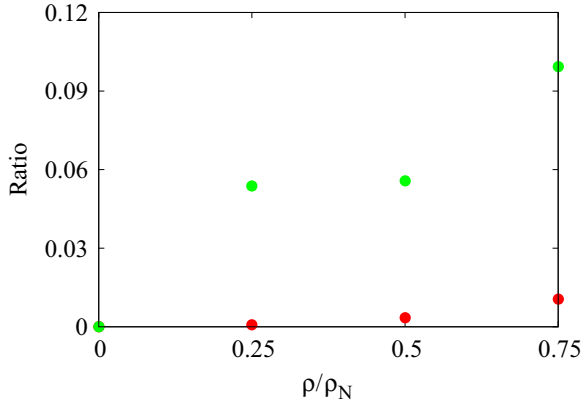
FIG. 6. The red (green) point corresponds to the ratio of the coefficient of the second term to the first term of $\Pi_m^+(q_0, |\vec{q}|)$ [$\Pi_m^-(q_0, |\vec{q}|)$] in Eq. (25).

V. SUMMARY AND CONCLUSION

We have studied the spectral functions of the nucleon and its negative-parity excited state in nuclear matter by using QCD sum rules and the maximum entropy method. All known first-order α_s corrections to the Wilson coefficients are taken into account and the density dependencies of the condensates are treated within the linear density approximation. With these inputs, we have constructed the parity-projected in-medium nucleon QCD sum rules and have analyzed them with the MEM. As a result, we have found that the density dependencies of the OPE parts are dominated by those of the chiral condensate $\langle \overline{q}q \rangle$ and vector quark condensate $\langle q^\dagger q \rangle$. The difference between the positive- and negative-parity OPE expressions is mainly caused by the chiral condensate term, whose sign depends on the parity of the respective nucleon state. Therefore, the density dependencies of the positive- and negative-parity OPE parts are rather different. As the density increases, the positive-parity OPE decreases rapidly because the in-medium modifications of $\langle \overline{q}q \rangle$ and $\langle q^\dagger q \rangle$ are added up to reduce the OPE part. On the other hand, the negative-parity OPE depends little on the density due to the cancellation of these modifications.

We have analyzed these OPE data by MEM and extracted the spectral functions of positive- and negative-parity, which in the vacuum exhibit sharp peaks near the experimental values of the lowest-lying states. The positions of these peaks turned out to be almost density independent, which means that the total energies of both the positive- and negative-parity states are not modified by nuclear matter effects up to normal nuclear matter density. On the other hand, as the density increases, the residue of the positive-parity nucleon ground state decreases while that of the negative-parity first-excited state remains almost unchanged.

Assuming mean-field type phenomenological nucleon propagators, we have next investigated the density dependencies of the effective masses and vector self-energies. For positive-parity, we have found that, as the density increases, the effective mass decreases while the vector self-energy increases. For negative parity, the medium modifications of these quantities are very small. We have examined potential effects of the uncertainties of the input parameters; namely, the in-medium four-quark condensates $\langle \overline{q}q \rangle_m^2$ and the chiral condensate $\langle \overline{q}q \rangle_m$, on the results of the analyses. It is found that these uncertainties mainly affect the effective mass and vector self-energy of the positive-parity ground state. For larger in-medium modifications of these condensates, the effective mass and vector self-energy become more pronounced. These results suggest that the effective mass and vector self-energy are strongly correlated with the partial restoration of chiral symmetry. For negative parity, the in-medium modifications are not much affected by the density dependencies of both $\langle \overline{q}q \rangle$ and $\langle \overline{q}q \rangle^2$, which suggests that the results qualitatively do not depend on our specific choices for the in-medium condensates. We have also investigated the spatial momentum dependence of the nucleon spectra and found that the $|\vec{q}|$ dependence of the total energies, the effective masses, and vector self-energies of both positive and negative parity are small at low density. Here, we have restricted ourselves to momenta up to the Fermi momentum at normal nuclear matter density. We have also discussed the validity of the parity projection at finite $|\vec{q}|$ and showed that, even though parity projection is not exact at finite $|\vec{q}|$, the mixing contributions of opposite parity states are sufficiently small up to the Fermi momentum.

The behavior of the positive- and negative-parity states can be attributed mainly to the modifications of the $\langle \overline{q}q \rangle$ and $\langle q^\dagger q \rangle$ condensates and thus our results indicate that both the $\langle \overline{q}q \rangle$ and $\langle q^\dagger q \rangle$ condensates are important in describing the in-medium properties of the nucleon and its negative-parity excited state. It is, however, difficult to provide an intuitive physical interpretation for these findings. Our results show that the spectral function, effective mass, and vector self-energy of the negative-parity state are not modified significantly up to normal nuclear matter density. This behavior differ from that obtained from the chiral doublet model, which predicts that the effective masses of both the positive- and negative-parity states decrease monotonically and finally become degenerate in the chirally restored phase. As a further point, the decrease of the peak height of the positive-parity spectral function indicates that the coupling strength of the nucleon ground state to the interpolating field is reduced rapidly as the density increases. These new features of the direct application of QCD are quite interesting, while their physical picture is not yet clear and requires further investigation.

[1] S. Weinberg, Phys. Rev. **177**, 2604 (1969).
[2] C. DeTar and T. Kunihiro, Phys. Rev. D **39**, 2805 (1989).
[3] D. Jido, Y. Nemoto, M. Oka, and A. Hosaka, Nucl. Phys. A **671**, 471 (2000).
[4] Q. Haider and L. C. Liu, Phys. Lett. B **172**, 257 (1986).
[5] H. C. Chiang, E. Oset, and L. C. Liu, Phys. Rev. C **44**, 738 (1991).
[6] D. Jido, H. Nagahiro, and S. Hirenzaki, Phys. Rev. C **66**, 045202 (2002).
[7] H. Nagahiro, D. Jido, and S. Hirenzaki, Phys. Rev. C **80**, 025205 (2009).
[8] E. Friedman, A. Gal, and J. Mareš, Phys. Lett. B **725**, 334 (2013).
[9] R. E. Chrien *et al.*, Phys. Rev. Lett. **60**, 2595 (1988).
[10] M. Pfeiffer *et al.*, Phys. Rev. Lett. **92**, 252001 (2004).
[11] A. Budzanowski *et al.*, Phys. Rev. C **79**, 012201 (2009).
[12] M. A. Shifman, A. Vainshtein, and V. I. Zakharov, Nucl. Phys. B **147**, 385 (1979).
[13] M. A. Shifman, A. Vainshtein, and V. I. Zakharov, Nucl. Phys. B **147**, 448 (1979).
[14] B. L. Ioffe, Nucl. Phys. B **188**, 317 (1981).
[15] N. Krasnikov, A. Pivovarov, and N. Tavkhelidze, Z. Phys. C: Part. Fields **19**, 301 (1983).
[16] Y. Chung, H. G. Dosch, M. Kremer, and D. Schall, Z. Phys. C: Part. Fields **25**, 151 (1984).
[17] M. Jamin, Z. Phys. C: Part. Fields **37**, 635 (1988).
[18] A. Ovchinnikov, A. Pivovarov, and L. Surguladze, Int. J. Mod. Phys. A **6**, 2025 (1991).
[19] H. Shiomi and T. Hatsuda, Nucl. Phys. A **594**, 294 (1995).
[20] V. A. Sadovnikova, E. G. Drukarev, and M. G. Ryskin, Phys. Rev. D **72**, 114015 (2005).
[21] V. M. Belyaev and B. L. Ioffe, Zh. Eksp. Teor. Fiz. **83**, 876 (1982) [Sov. Phys. JETP **56**, 493 (1982)].
[22] D. B. Leinweber, Ann. Phys. (NY) **198**, 203 (1990).
[23] Y. Chung, H. G. Dosch, M. Kremer, and D. Schall, Nucl. Phys. B **197**, 55 (1982).
[24] D. Jido, N. Kodama, and M. Oka, Phys. Rev. D **54**, 4532 (1996).
[25] Y. Kondo, O. Morimatsu, and T. Nishikawa, Nucl. Phys. A **764**, 303 (2006).
[26] K. Ohtani, P. Gubler, and M. Oka, Phys. Rev. D **87**, 034027 (2013).
[27] T. Hatsuda, H. Høgaasen, and M. Prakash, Phys. Rev. Lett. **66**, 2851 (1991).
[28] T. Hatsuda and S. H. Lee, Phys. Rev. C **46**, R34 (1992).
[29] K. S. Jeong, G. Gye, and S. H. Lee, arXiv:1606.00594.
[30] E. G. Drukarev and E. M. Levin, Nucl. Phys. A **511**, 679 (1990).
[31] T. Cohen, R. Furnstahl, D. Griegel, and X.-m. Jin, Prog. Part. Nucl. Phys. **35**, 221 (1995).
[32] E. G. Drukarev, M. G. Ryskin, and V. A. Sadovnikova, Phys. At. Nucl. **75**, 334 (2012).
[33] P. Gubler and M. Oka, Prog. Theor. Phys. **124**, 995 (2010).
[34] K. Ohtani, P. Gubler, and M. Oka, Eur. Phys. J. A **47**, 114 (2011).
[35] P. Gubler, K. Morita, and M. Oka, Phys. Rev. Lett. **107**, 092003 (2011).
[36] K.-J. Araki, K. Ohtani, P. Gubler, and M. Oka, Prog. Theor. Exp. Phys. (2014) 073B03.
[37] P. Gubler and K. Ohtani, Phys. Rev. D **90**, 094002 (2014).
[38] S. Groote, J. G. Korner, and A. A. Pivovarov, Phys. Rev. D **78**, 034039 (2008).
[39] T. D. Cohen, R. J. Furnstahl, and D. K. Griegel, Phys. Rev. C **45**, 1881 (1992).
[40] N. Kaiser, P. de Homont, and W. Weise, Phys. Rev. C **77**, 025204 (2008).
[41] S. Goda and D. Jido, Phys. Rev. C **88**, 065204 (2013).
[42] S. Borsanyi, S. Durr, Z. Fodor, S. Krieg, A. Schafer, E. E. Scholz, and K. K. Szabo, Phys. Rev. D **88**, 014513 (2013).
[43] K. A. Olive *et al.* (Particle Data Group), Chin. Phys. C **38**, 090001 (2014).
[44] P. Colangelo and A. Khodjamirian, *At the Frontier of Particle Physics: Handbook of QCD* (World Scientific, Singapore, 2001), Vol. 3, p. 1495.
[45] X. Jin, M. Nielsen, T. D. Cohen, R. J. Furnstahl, and D. K. Griegel, Phys. Rev. C **49**, 464 (1994).
[46] A. Martin, W. Stirling, R. Thorne, and G. Watt, Eur. Phys. J. C **63**, 189 (2009).
[47] P. Gubler, K. S. Jeong, and S. H. Lee, Phys. Rev. D **92**, 014010 (2015).
[48] M. Asakawa, T. Hatsuda, and Y. Nakahara, Prog. Part. Nucl. Phys. **46**, 459 (2001).
[49] R. N. Silver, J. E. Gubernatis, D. S. Sivia, and M. Jarrell, Phys. Rev. Lett. **65**, 496 (1990).
[50] D. B. Leinweber, Ann. Phys. (NY) **254**, 328 (1997).
[51] B. D. Serot and J. D. Walecka, Adv. Nucl. Phys. **16**, 1 (1986).
[52] B. D. Serot, Rep. Prog. Phys. **55**, 1855 (1992).
[53] Y. Kwon, M. Procura, and W. Weise, Phys. Rev. C **78**, 055203 (2008).
[54] P. Gubler and W. Weise, Phys. Lett. B **751**, 396 (2015).
[55] R. Thomas, T. Hilger, and B. Kampfer, Nucl. Phys. A **795**, 19 (2007).
[56] E. G. Drukarev, M. G. Ryskin, and V. A. Sadovnikova, Phys. Rev. C **86**, 035201 (2012).
[57] K. S. Jeong and S. H. Lee, Phys. Rev. C **87**, 015204 (2013).
[58] P. E. Shanahan, A. W. Thomas, and R. D. Young, Phys. Rev. D **87**, 074503 (2013).
[59] J. M. Alarcon, J. M. Camalich, and J. A. Oller, Phys. Rev. D **85**, 051503 (2012).
[60] S. Durr *et al.*, Phys. Rev. D **85**, 014509 (2012).
[61] B. Blossier *et al.*, Phys. Rev. D **82**, 114513 (2010).
[62] S. Durr *et al.*, Phys. Lett. B **701**, 265 (2011).
[63] Y. Aoki *et al.*, Phys. Rev. D **83**, 074508 (2011).
[64] M. Hoferichter, J. Ruiz de Elvira, B. Kubis, and Ulf-G. Meißner, Phys. Rev. Lett. **115**, 092301 (2015).
[65] S. Durr *et al.*, Phys. Rev. Lett. **116**, 172001 (2016).